Grain boundary segregation of C, N and O in hexagonal close-packed titanium from first principles

Article *in* Modelling and Simulation in Materials Science and Engineering · September 2013

DOI: 10.1088/0965-0393/21/7/075009

3 authors, including:

D.A. Aksyonov
Skolkovo Institute of Science and Technology
15 PUBLICATIONS **40** CITATIONS
SEE PROFILE

Yuriy Romanovich Kolobov
Belgorod State University
216 PUBLICATIONS **1,373** CITATIONS
SEE PROFILE

Grain boundary segregation of C, N and O in hexagonal close-packed titanium from first principles

2013 Modelling Simul. Mater. Sci. Eng. 21 075009

(http://iopscience.iop.org/0965-0393/21/7/075009)

Modelling Simul. Mater. Sci. Eng. **21** (2013) 075009 (12pp) doi:10.1088/0965-0393/21/7/075009

Grain boundary segregation of C, N and O in hexagonal close-packed titanium from first principles

D A Aksyonov, A G Lipnitskii and Yu R Kolobov

Center of Nanostructured Materials and Nanotechnologies, Belgorod State University, Belgorod, Russia

Received 17 May 2013, in final form 30 July 2013
Published 18 September 2013
Online at stacks.iop.org/MSMSE/21/075009

Abstract
Grain boundary segregation of light interstitials is one possible mechanism of thermal stability in commercially pure nanostructured titanium alloys. This paper uses first-principles calculations to show that the independent segregation of C, N and O atoms at a $\Sigma 7$ high angle grain boundary in α-Ti is energetically unfavourable. The presence of interstitial elements near the grain boundary plane increases the grain boundary width and the specific formation energy.

(Some figures may appear in colour only in the online journal)

1. Introduction

An increase or decrease in the concentration of impurities at grain boundaries (GBs), also known as segregations, can considerably influence various properties of polycrystalline materials [23]. In addition to causing an embrittlement effect, these changes can increase GB cohesion and significantly improve the thermal stability of nanocrystalline materials [4, 6–8, 10, 24,29, 38, 41, 44, 45]. Therefore, in the design and optimization of nanomaterials, which have a large specific area of interfaces that can give rise to segregations, it is important to understand the influence of segregations on material properties.

Commercially pure nanostructured α-titanium (CP-nTi) alloys with hexagonal close packed (hcp) lattice structures exhibit a high biocompatibility and superior strength in comparison with coarse-grained Ti [15, 17]. As CP-nTi is a promising material for lifetime medical and dental implants, thermal stability is a critical parameter. There are no data in the literature about the long-term behaviour of this material because the mechanisms that thermally stabilize nTi are not yet understood. Because implants must be heat treated during production for technical reasons, the improvement of their microstructural stability is an important task. A detailed understanding of the existing mechanisms of GB stabilization is required to approach this problem. CP titanium alloys (grades 1–4) contain sufficiently large amounts of light element impurities, such as C, N and O [17]. Thus, two mechanisms of thermal stability are possible in nTi: (i) GB pinning by precipitates (dispersed particles of carbides, nitrides, etc formed from solid solution) and (ii) a decreased driving force for grain growth and a reduction in the GB mobility due to the segregation of existing impurities [44]. Our recent

work considered the possibility of the formation of Ti–C precipitates in α-Ti [2]. The purpose of the current work is to continue the investigation of the mechanisms of thermal stability in CP-nTi, considering light impurity segregation at α-Ti GBs, and to compare these results with previous results on Ti–C particle formation.

Semenova *et al* [35] have recently observed elevated concentrations of C, N and O at GBs in CP-nTi by atomic probe tomography, confirming that the segregation of light elements at α-Ti GBs is possible. However, no clear conclusions can be made about their influence on material properties because many factors act together. Does the segregation correspond to an equilibrium state? Do elements co-segregate? Is the formation of clusters at GBs favourable? How strong are the interactions between the impurities and the GB? While it is difficult or even impossible to answer these questions with solely experimental methods, computer simulations can provide insight [26]. Recently, studies of segregation from first principles have become more common [1, 3, 9, 11, 12, 18, 21, 25, 31, 33, 34, 39, 40, 42, 46, 47], but no such studies have been reported for hcp metals. This work aims to fill this gap using the example of hcp titanium.

In summary, this study of segregation in Ti will allow us to take further steps towards discovering the most effective mechanism of improving the thermal stability of CP-nTi. Note that molecular dynamics and Monte Carlo simulations are the most efficient tools for quantitative studies of the thermal stability of GB structures, including the kinetic details. However, these methods are based on empirical interatomic potentials, and therefore, they must be benchmarked with first-principles calculations (which are currently not available [26]. These calculations are based on the determination of segregation formation energies for the diffusion of the impurity atom from a bulk site to a GB site.

Thus, this paper investigates the interactions of C, N and O impurities with a $\Sigma 7[0\,0\,0\,1](1\,2\,\bar{3}\,0)$ GB in α-Ti from first principles. The results include the segregation energies of impurities for different positions near and at the GB plane. The influence of impurities on the GB is accounted for by the relaxation of the atomic structure of the GB. We analyse the electronic structure to explain several features of the interactions between the GB and impurities.

2. Details of calculation

Calculations of the full energies and optimized geometries were performed using the density-functional theory (DFT) framework [16, 20] within the generalized gradient approximation (GGA) using the Perdew–Burke–Wang [30] functional and projected augmented wave (PAW) method [5] (ABINIT [13]). We considered the following valence electronic states: 3s, 3p, 4s, 3d for Ti and 2s, 2p for C, N and O. To remove any restrictions during relaxation, we set the number of point group symmetry operations to one in all cases. The calculations were performed under three-dimensional periodic boundary conditions. An orthorhombic supercell containing 56 Ti atoms was constructed using the theoretical lattice constants for a primitive hcp titanium cell, which were calculated in our previous work [2]. The cell volume was subsequently relaxed to take into account the influence of cell size and to refine the lattice constant values. The resulting supercell containing 54 Ti atoms was used as a starting model for the $\Sigma 7[0\,0\,0\,1](1\,2\,\bar{3}\,0)$ GB [14, 32] (figure 1). To determine the optimal GB geometry, the supercell was relaxed with fixed dimensions (as for bulk Ti) in the plane of the GB.

The sizes of supercells and the lengths $d_{\mathrm{Ti–Ti}}$ between Ti atoms in the $[1\,0\,\bar{1}\,0]$ direction (coinciding with the a lattice constant in the case of bulk Ti) are listed in table 1. The value of $d_{\mathrm{Ti–Ti}}$ for the bulk Ti supercell is in agreement with the experimental lattice constant. In the case of the supercell with GBs, the variation of $d_{\mathrm{Ti–Ti}}$ is caused by the influence of GBs and is related to the finite cell size. However, recent studies confirmed that the cell sizes selected here

Table 1. Specific excess energy γ (J m^{-2}) of GBs before and after relaxation for supercells of sizes a, b and c (Å), distance $d_{\mathrm{Ti–Ti}}$ (Å) between Ti atoms in the [1 0 $\bar{1}$ 0] direction.

Cell	γ	a	b	c	$d_{\mathrm{Ti–Ti}}$
$\mathrm{Bulk_{relax}}$	—	7.77	27.03	4.62	2.95
$\mathrm{GB_{ideal}}$	1.8	7.77	27.03	4.62	2.95
$\mathrm{GB_{relax}}$	0.73	7.77	25.97	4.62	2.75–3.25

are sufficient to describe the GB structures of hexagonal materials [22] and GB segregation energies [33].

To study the interactions of impurities with the GB, we placed atoms at different positions in the optimized supercell and relaxed the cell by adjusting all internal coordinates and the size of the supercell in the direction perpendicular to the GB plane. The calculations were performed using an energy cut-off of 540 eV for the plane-wave basis set. The Brillouin-zone (BZ) integrals were approximated using the special k-point sampling of Monkhorst and Pack [28] with a $2 \times 1 \times 4$ grid. We used Methfessel–Paxton [27] smearing for BZ integration with a smearing width of 0.027 eV. This relatively small value does not influence the results but ensures faster convergence. The structural optimization was performed until the forces acting on each atom were less than 25 meV Å^{-1}. The computational setup ensures that differences in the segregation energies of interstitial atoms and in the formation energies of Ti GBs converge to within 25 meV and 0.05 J m^{-2}, respectively. The calculation method and the Ti–C PAW potentials were checked by calculating the lattice and elastic constants of several Ti and Ti–C phases in our previous study [2].

3. Results and discussion

3.1. Structure and energy of the pure GB

Periodic and free boundary conditions (PBC and FBC) are mainly used for GB modelling. Free boundary conditions enable one GB to be examined in a simulation cell at the cost of adding two open surfaces. This approach is useful for cells with two non-equivalent GBs. However, open surfaces exert a significant influence on the atomic structure of the supercell. The attempt to reduce this influence by introducing fixed layers leads to additional restrictions on the relative movement between adjacent grains during relaxation. In this work, despite the existence of two non-equivalent GBs in the simulation cell, we use periodic boundary conditions to avoid difficulties related to open surfaces. This approach is reasonable due to the specific atomic configuration of the cell, with one fully coherent GB obtained after relaxation.

The ideal symmetric coincident-site lattice (CSL) GB $\Sigma 7[0\,0\,0\,1](1\,2\,\bar{3}\,0)$ with $\varphi_{\mathrm{CSL}} = 21.8^{\circ}$ is used as the initial GB structure. This boundary perfectly agrees with experimentally observed GBs in α-Ti [43]. The procedure by which this GB was constructed is described elsewhere [14]. After the mathematical construction of the supercell, two pairs of atoms lie too close to each other. Thus, according to [14], each pair was replaced with a single atom.

Two simulation cells are shown in figure 1(*a*) to indicate the structure of both GBs. Ti atoms in the bulk regions and at GBs are shown with different colours to guide the eye. The atomic configurations at the G1 and G2 GBs (see figure 1(*a*)) are pentagonal in both layers, which is consistent with the minimum binding energy structure obtained in [14]. However, differences exist between the structures of G1 and G2 in the bottom layer A (see figure 1(*a*)). The pentagon in this layer at G2 is stretched in the [1 2 $\bar{3}$ 0] direction relative to the pentagon at the G1 GB. Moreover, the upper pentagon at G2 is shifted relative to the bottom pentagon

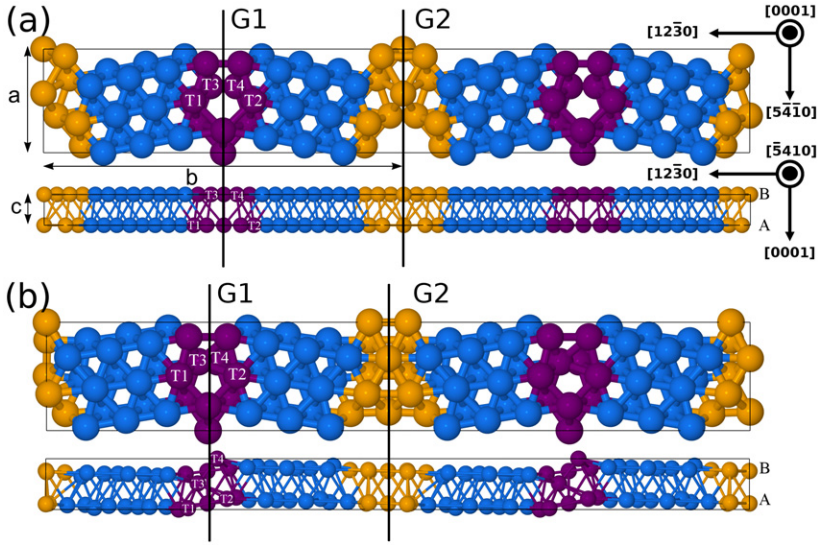

Figure 1. (*a*) Structure of the supercell with Σ7 GBs after mathematical construction. (*b*) Structure of the supercell with Σ7 GBs after the full relaxation. The grain shift is clearly visible. Two simulation cells are shown to illustrate the structure of the second GB. The atoms are coloured differently to distinguish between atoms at the GB and in the bulk. The solid lines G1 and G2 denote GB planes.

in the $[5\,\bar{4}\,\bar{1}\,0]$ direction compared with the G1 structure. These differences arise from the fact that the CSL only exists in layer B for the given rotation angle.

Two simulation cells after relaxation are shown in figure 1(*b*). The main difference between these cells and the non-relaxed structure is that the grains are shifted relative to each other along the $[0\,0\,0\,1]$ direction. The interesting feature is that this shift only occurs at G1 and not at G2. The values of the shifts, Δr_1 in the $[5\,\bar{4}\,\bar{1}\,0]$ direction and Δr_2 in the $[0\,0\,0\,1]$ direction, are averaged among several atoms in the bulk region of the grains and calculated relative to the initial state. Almost no shift occurs in the $[5\,\bar{4}\,\bar{1}\,0]$ direction for the pure relaxed GB, while the value of Δr_2 is 0.45 Å.

The atomic structure of the G1 and G2 GBs was also significantly changed after relaxation. In the case of the G1 GB, T3 and T4 atoms are shifted in opposite directions, breaking the symmetry of the pentagon and forming a closer packed configuration that is more preferable for titanium. The relaxation leads to a 3.7% reduction in cell size in the $[1\,2\,\bar{3}\,0]$ direction (see table 1).

The atomic structure of G2 is highly symmetrical. The visual analysis indicates the presence of the ω-Ti phase [36] at G2. The conventional cell of ω-Ti carved out from G2 is shown in figure 2, where the marked Ti atoms match with figure 1. The orientation relationship is $(0\,0\,0\,1)_\alpha \parallel (1\,\bar{2}\,1\,0)_\omega$ and $[1\,2\,\bar{3}\,0]_\alpha \parallel [0\,0\,0\,1]_\omega$, which agrees with the Silcock [37] relationship for planes but differs for directions ($[1\,1\,\bar{2}\,0]_\alpha \parallel [0\,0\,0\,1]_\omega$ for Silcock). We did not find experimental confirmation of such $[1\,2\,\bar{3}\,0]_\alpha \parallel [0\,0\,0\,1]_\omega$ relationships for directions, but the obtained $\omega - \alpha$ interfaces are quite coherent. The lattice parameters of the ω-Ti phase at the GB are in agreement with those for bulk ω-Ti calculated in [2]. The interface period in the $[0\,0\,0\,1]$ direction (4.62 Å) matches very well with the a parameter of the bulk ω-Ti (4.58 Å). The period in the $[5\,\bar{4}\,\bar{1}\,0]$ direction (7.77 Å) matches well with $\sqrt{3}a$ in the bulk ω-Ti (7.92 Å).

Therefore, we justify the choice of PBC by the assumption that the influence of the coherent G2 GB on the structure of the G1 GB is less than that of the open surfaces in the framework

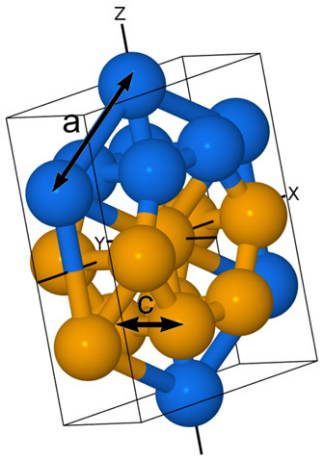

Figure 2. The structure of the G2 GB. The marked atoms correspond to those in figure 1. The additional atoms, obtained by periodic replication, complete the conventional cell of the ω-Ti phase in the GB. Here, a and c correspond to the lattice parameters of ω-Ti. The z- and y-axes coincide with the [0 0 0 1] and [1 2 $\bar{3}$ 0] directions.

of free boundary conditions. The use of PBC enables automatic relative grain shifts at G1 as the coherent G2 GB does not restrict the lateral shifts.

As the G1 and G2 GBs are not equivalent, the following equation allows for the calculation of the specific excess energy related to the GBs:

$$\gamma = [E_{\mathrm{GB}}(n, a, c) - nE_{\mathrm{sub}}(1, a, c)]/S, \tag{1}$$

where $E_{\mathrm{GB}}(n, a, c)$ is the energy of the cell with GBs and n Ti atoms, $E_{\mathrm{sub}}(1, a, c)$ is the energy of one atom in the commensurate Ti hcp bulk supercell, and $S = 2ac$. The values of γ for the GBs considered before and after relaxation are listed in table 1. The specific excess GB energy was decreased by more than two times after relaxation.

GB segregation was investigated further for the high-angle G1 GB.

3.2. Positions of C, N and O atoms

To study the interactions of impurities with the G1 GB, the same positions are used for the C, N and O atoms. We have considered five different interstitial positions within the simulation cell: $X1$ at the G1 GB (X = C, N, O) and $X2$–$X5$ at several distances from the G1 plane. The resulting configurations of all atoms are also named by Xi later in the text. The locations of these positions are shown within one relaxed simulation cell in figure 3 as the corresponding atomic configurations after relaxation are quite similar for all cases. The $X2$–$X5$ positions correspond to slightly deformed octahedral pores, while the pore at the $X1$ position has a more complicated topology.

We performed additional full relaxation to take the possible influence of impurities on the GB structure into account. Table 2 reports the distance d from the G1 plane to the impurities after relaxation. The $X5$ position at the centre of the two GBs is considered the reference state of impurities in the titanium bulk.

The concentration of interstitials within the grain bulk is 1.8 at%. The solute excess of interstitials within the GB plane is 4.63×10^{-6} mole m^{-2}, which is a typical value of solute excess of interstitials in metals.

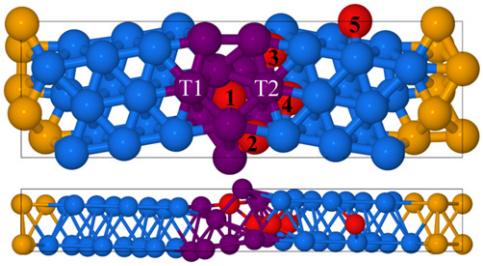

Figure 3. Atoms 1–5 indicate the initial positions used for C, N and O within one relaxed simulation cell.

Note that the distance between the impurity and its periodic image in the [0 0 0 1] direction is quite small and that some interaction is possible. However, we found that after the supercell doubling in the [0 0 0 1] direction, the energy of carbon atom in the octahedral site (the difference between the energy of the titanium supercell with one carbon atom and that of the same supercell without a carbon atom) is reduced only by 60 meV. As the energy change is only 10% of the C1 segregation energy (provided below), the related interaction between impurity and its image can be neglected. Moreover, this interaction is reduced during the calculation of segregation energies and does not influence their values directly.

3.3. Segregation energies and volumes of C, N and O atoms at the α-Ti GB

The stability of GBs depends on their energies of formation [44]. It is well established that the reduction in the GB specific energy due to the segregation of some impurities can significantly improve the thermal stability of the nanostructure [7, 19].

To determine the possible decrease in GB energy due to impurities, the segregation energies and volumes of the C, N and O atoms at the $\Sigma 7[0\,0\,0\,1](1\,2\,\bar{3}\,0)$ CSL GB in α-Ti were calculated at 0 K according to the following equations:

$$\begin{aligned} E_{\text{seg}} &= E_{Xi} - E_{X5}, \\ V_{\text{seg}} &= V_{Xi} - V_{X5} \end{aligned}, \tag{2}$$

where E_{Xi} and V_{Xi} represent the energy and volume of the simulation cell with atom X at position i, and E_{X5} and V_{X5} are the energy and volume, respectively, of the same simulation cell with atom X occupying an interior grain site. The segregation energies and volumes are listed in table 2. The same trends can be derived for C, N and O. The segregation of impurities is unfavourable near the $\Sigma 7$ GB in all considered positions. Moreover, the preference of positions decreases towards the G1 GB plane (see figure 4). The segregation energies for the same positions exhibit almost no dependence on the type of impurity, indicating that C, N and O interact with the $\Sigma 7$ GB in a similar way for α-Ti. The increase in the segregation energy is accompanied by an increase in the segregation volume. The increase in the cell volume is related to the expansion of the G1 GB. In particular, the distances between the T1 and T2 atoms are 4.23 Å for C5, 4.32 Å for C3 and 4.53 Å for the C1 configuration.

The relative grain shifts are listed in table 2. The values of shifts Δr_1 in the $[5\,\bar{4}\,\bar{1}\,0]$ direction are quite small (less than 5% of the titanium lattice constant) and are not significant. However, grains have noticeable additional shifts in the [0 0 0 1] direction at the G1 plane due to the presence of impurities. The maximum shift is observed for the $X3$ configuration, which is up to 30% greater than Δr_2 in the pure GB. The dependence of the shifts on the position of

Table 2. Segregation energy E_{seg} (eV) and its separation into mechanical E_m and chemical E_{ch} contributions. Geometric data include the lateral grain shifts Δr_1 in the $[5\,\bar{4}\,\bar{1}\,0]$ direction and Δr_2 in the [0 0 0 1] direction (Å), the distance d (Å) between the impurity and the G1 grain boundary plane, and the segregation volume V_{seg} (Å^3) for all considered configurations. The C5, N5 and O5 configurations have the same parameters and are denoted $X5$.

	C1	N1	O1	C2	N2	O2	C3	N3	O3	C4	N4	O4	$X5$
Δr_1	0.14	0.16	0.18	−0.08	−0.07	−0.08	0.08	0.07	0.08	0.06	0.07	0.06	0.04
Δr_2	0.41	0.49	0.50	0.34	0.33	0.37	0.53	0.50	0.42	0.38	0.48	0.42	0.34
d	0.16	0.35	0.35	1.44	1.44	1.44	2.46	2.49	2.51	3.34	3.32	3.33	7.25
E_{seg}	0.66	0.72	0.68	0.23	0.30	0.31	0.36	0.49	0.46	0.13	0.18	0.21	0.00
E_m	0.96	0.35	0.27	0.12	0.13	0.12	0.19	0.24	0.21	0.04	0.04	0.06	0.00
E_{ch}	−0.29	0.37	0.40	0.11	0.17	0.19	0.17	0.25	0.25	0.09	0.15	0.16	0.00
V_{seg}	8.03	4.10	3.26	2.92	4.02	3.09	0.90	3.78	2.67	0.13	1.28	1.51	0.00

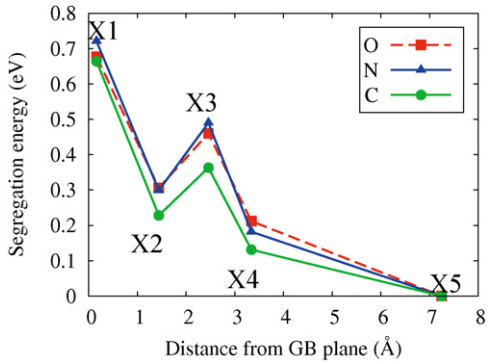

Figure 4. Dependence of segregation energy E_{seg} on the position of the impurity.

the impurity is rather complex; however, in most cases, larger shifts are associated with larger E_{seg} values.

To gain more physical insight into the similarities of segregation energies among different elements, we separated E_{seg} into mechanical and chemical contributions according to Geng *et al* [12] as follows. The mechanical contribution E_m was determined as the difference in the energy of the structure resulting from the removal of the impurity without subsequent relaxation of the host lattice. In other words, E_m is related to the Ti–Ti interaction induced by the impurity. The chemical contribution

$$E_{ch} = E_{seg} - E_m \tag{3}$$

describes the direct interaction between the impurity and Ti atoms. The calculated values of E_m and E_{ch} are listed in table 2. For all configurations besides C1, the following regularities are observed. (i) The chemical contribution dominates over E_m and correlates with E_{seg}. (ii) Different elements at the same positions make very similar contributions. (iii) The positive values of E_m for positions $X2$–$X4$ are related to the changes in the arrangement of Ti at the GB and the additional deformation of octahedral pores near the G1 GB. (iv) The positive values of E_{ch} are also related to the deformation of octahedral pores and the depletion of charge density near the GB. In general, elements such as C, N and O behave in a similar way. The segregation energy at the C1 position, which exhibits a negative chemical contribution, is of particular interest and will be discussed below.

To explain the positive values of the segregation energies, we have studied the electronic structure and the distribution of the charge density. The line profile of the charge density

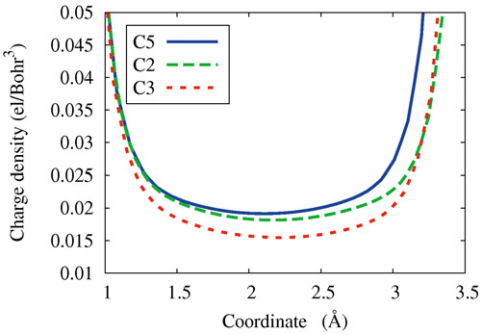

Figure 5. Line profile of the charge density between the T1 (0 Å) and T2 (4.22 Å) atoms for the case of carbon segregation at positions C5, C2 and C3. The profile for C4 is just below that for C5 and is not shown. The C1 profile is much higher than the C5 profile due to the location of the carbon atom and is also not shown.

between atoms T1 and T2 is shown in figure 5 for the case of carbon. Further discussion will focus on X impurity because all three elements exhibit the same behaviour. Carbon, nitrogen and oxygen tend to form covalent spd-bonds with Ti atoms, accompanied by the redistribution of the charge density, accumulation between Ti–X atoms and depletion between neighbouring Ti–Ti atoms. For $X2$, $X3$ and, to a lower extent, $X4$, this redistribution affects the GB region. The depletion of the charge density between atoms T1 and T2 results in a weakening of Ti bonds at the G1 GB, increasing their length and increasing the width of the G1 GB. The increase in the GB width and volume results in higher segregation volumes and energies. The density between T1 and T2 is the highest for the $X1$ position due to the location of the impurity, but the atomic size effect leads to the greatest GB width and the highest segregation energy among all positions.

Kwasniak *et al* recently deduced from first principles that C, N and O decrease the formation energies of stacking faults in α-Ti, which means that the segregation of these elements at stacking faults is energetically favourable. However, these authors did not explain the physical reasons for this behaviour. Stacking faults have smaller formation energies than high-angle GBs. Trelewicz and Schuh [39], within the framework of statistical thermodynamics, showed that in binary polycrystalline systems, the segregation energy decreases (increases for the choice of the sign of E_{seg} in [39]) as the GB formation energy decreases. Thus, the segregation of C, N and O is possible at low-energy interfaces in α-Ti but is hardly feasible at high-angle GBs with large formation energies.

3.3.1. The features of GB segregation. The dependence of the segregation energy on position in figure 4 exhibits a pronounced peak for the $X3$ configuration. The impurity at the $X3$ position is slightly further (by 1 Å) from the GB plane than the impurity at the $X2$ position, leading to a greater segregation energy. This result can be understood as follows: the impurity at the $X3$ position attracts the T4 titanium atom (see figure 1), reducing the T3–T4 spacing. The GB tends to conserve the T3–T4 spacing, leading to an additional shift of grains in the [0 0 0 1] direction (see table 2). In turn, the impurity at the $X2$ position does not affect the arrangement of Ti atoms at the GB and preserves the same shift as in the reference $X5$ position. As a consequence, the additional disturbance of the GB structure by the impurity at the $X3$ position results in a higher segregation energy than the impurity at the $X2$ position.

Nevertheless, the segregation of carbon at the C1 position (directly at the GB) is unfavourable, with a negative chemical contribution to segregation energy observed

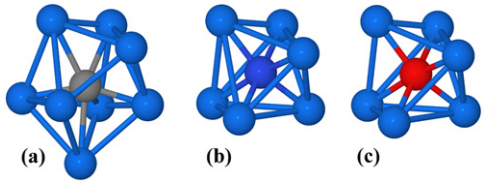

Figure 6. Local coordination of interstitial sites at the GB for C1 (*a*), N1 (*b*) and O1 (*c*). There are eight Ti neighbours in the case of carbon and only six in the cases of nitrogen and oxygen.

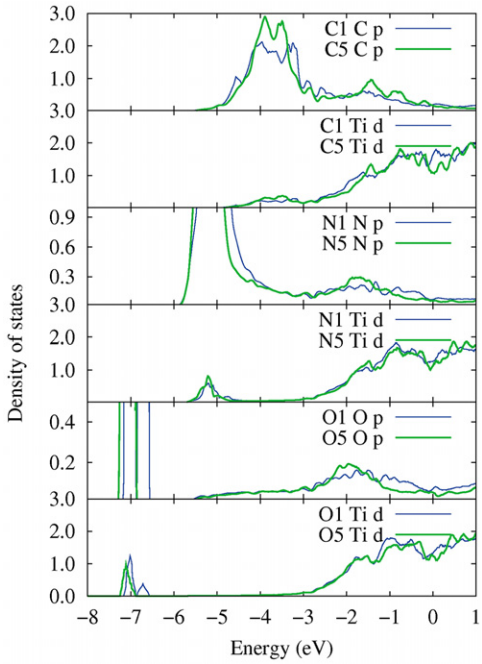

Figure 7. Site-projected PDOS of impurities and surrounding titanium atoms for the $X1$ and $X5$ positions. The Fermi level lies at zero energy.

(see table 2). This means that the work needed to remove the carbon without permitting the Ti atoms to relax from the C1 position is 0.29 eV greater than that for C5. The comparisons among C1, N1 and O1 shows that in the case of C1, the surrounding Ti coordination is more complex, consisting of eight Ti neighbours. The local environments of atoms obtained from GBs are shown in figure 6. The local coordinations of the N1 and O1 positions are distorted octahedral sites with six Ti neighbours. The local coordination of C1 is unique for this GB and could not be found in any known Ti carbide.

The restructuring of the interstitial site in the case of carbon may be related to its higher valency and chemical capacity to form bonds compared with N and O. However, due to the significant rearrangement of the GB structure, the loss in E_{m} overcomes the chemical gain.

To explain the reasons for the negative chemical contribution only in the case of carbon, we calculated the site-projected partial density of states (PDOS). The PDOS of the interstitial (p-orbitals) and surrounding Ti atoms (d-orbitals) for the $X1$ and $X5$ configurations are shown in figure 7. The PDOS of titanium for the $X1$ configuration was obtained by averaging over the Ti atoms shown in figure 6 and for the $X5$ configuration by averaging over the Ti atoms of the octahedral coordination around the impurity. The most notable differences in the PDOS

between the $X1$ and $X5$ positions are observed for carbon. For the majority of cases, the PDOS is consistent with the loss of energy for the case of the impurity at the $X1$ GB site: (i) the $X1$ PDOS shifts to higher energies relative to $X5$; (ii) the density of states decreases at several energies for the $X1$ case. However, the p states of carbon are qualitatively different between oxygen and nitrogen. In the case of carbon, the centre of gravity of p states at the $X1$ site is shifted to lower energies (−0.067 eV), while the centres of gravity of the N and O p bands at $X1$ are shifted to higher energies (+0.124 eV and +0.113 eV, respectively). This phenomenon can be related to the negative chemical contribution in the case of the C1 configuration.

The projected DOS of the Ti d states at the Fermi level for the C5 configuration (1.075) is lower than that for N5 and O5 (1.154 and 1.241, respectively), which may confirm more covalent nature of Ti–C bonds. Nevertheless, the DOS of the Ti d states at the Fermi level for C1 (1.641) is higher than the Ti d DOS of N1 and O1 (1.282 and 1.327, respectively). This is in agreement with the highest value of E_{m} for the C1 configuration. The smaller values of E_{m} for N and O are consistent with the lower values of V_{seg}, which means that the N and O atoms require less space at the GB than carbon.

In summarising these results, it should be mentioned that the method used to calculate E_{seg} has one drawback related to the optimization of the GB structure. This drawback is linked to the fact that it is difficult to determine the grain shifts that correspond to the global minimum of total energy by first principles. The compared configurations examined here could be relaxed to different local energy minima. However, this self-consistent picture of the interactions between impurities and GBs allows us to claim that the qualitative results will remain unchanged for the true ground states. Moreover, the quantitatively correct results have little sense for the case considered here as experimentally measured segregation energies are often averaged over a large number of sites at general GBs.

3.3.2. Comparison with experimental data. A few words should be said about the agreement between our results and experimental observations of increased concentrations of C, N and O at GBs in Ti by Semenova *et al* [35]. Primarily, we do not claim that equilibrium segregation of these elements is impossible in α-Ti in principle as we considered only one type of GB. However, we also suggest two interpretations for the experimental data. Semenova *et al* provide atom probe tomography composition profiles of interstitial impurities across the GB after annealing at 623 K (see figure 4 in [35]). On the one hand, the asymmetry and significant width of the observed concentration peaks are usually related to non-equilibrium segregation due to GB migration [23]. On the other hand, the correlation between peaks for carbon and oxygen suggests that C–O co-segregation was observed. Thus, there is an intriguing possibility of GB C–O co-segregation in α-Ti without independent segregation. Regarding the possible mechanisms of thermal stabilization in nanocrystalline pure titanium, the results of this work support GB pinning by bulk precipitates formed from solid solution [2].

4. Conclusions

In summary, we have investigated the interactions of C, N and O atoms with high-angle $\Sigma 7[0\,0\,0\,1](1\,2\,\bar{3}\,0)$ grain boundary (GB) in α-Ti through *ab initio* PAW potential calculations. The specific simulation cell with two non-identical GBs allowed us to use the full periodic boundary conditions due to the coherence of the second GB. The first GB has a structure of a non-symmetrical tilt boundary with lateral shifts, while the second GB replicates the structure of the ω-Ti phase with a $(0\,0\,0\,1)_\alpha \parallel (1\,\bar{2}\,1\,0)_\omega$ and $[1\,2\,\bar{3}\,0]_\alpha \parallel [0\,0\,0\,1]_\omega$ orientation relationship.

The segregation energies were calculated for different positions at different distances from the GB plane. All elements considered here exhibited similar behaviour and preferred to be in the octahedral site of bulk Ti. The maximum energy loss was observed for the positions at the GB interface. The analysis of the geometry and electronic structure showed that the increase in energy is due to the redistribution of the electronic density and due to a reduction in the bonding strength within the grain boundary area.

Therefore, we believe that thermal stability in nanostructured titanium is not controlled by the grain boundary segregation of the C, N and O impurities. However, we are aware that in a real system, more complex processes, such as grain boundary co-segregation and precipitation, could occur, making further theoretical and experimental investigations desirable.

Acknowledgments

The research that led to these results received funding from the Federal Target Program under Grant Agreement Nos 2.2437.2011 and 14.A18.21.0078. The authors are grateful to the 'SKIF-polytech' research group for providing computational resources on the 'SKIF Cyberia' cluster at Tomsk State University.

References

[1] Abbasi A, Dick A, Hickel T and Neugebauer J 2011 First-principles investigation of the effect of carbon on the stacking fault energy of Fe–C alloys *Acta Mater.* **59** 3041–8
[2] Aksyonov D A, Lipnitskii A G and Kolobov Yu R 2012 *Ab initio* study of Ti–C precipitates in hcp titanium: formation energies, elastic moduli and theoretical diffraction patterns *Comput. Mater. Sci.* **65** 434–41
[3] Astala R and Bristowe P D 2002 First principles calculations of niobium substitution in strontium titanate *J. Phys.: Condens. Matter* **14** L149
[4] Atwater M A, Scattergood R O and Koch C C 2013 The stabilization of nanocrystalline copper by zirconium *Mater. Sci. Eng.* A **559** 250–6
[5] Blochl P E 1994 Projector augmented-wave method *Phys. Rev.* B **50** 17953
[6] Choi P, Dasilva M, Klement U, Alkassab T and Kirchheim R 2005 Thermal stability of electrodeposited nanocrystalline Co–1.1 at%P *Acta Mater.* **53** 4473–81
[7] Chookajorn T, Murdoch H A and Schuh C A 2012 Design of stable nanocrystalline alloys *Science* **337** 951–4
[8] Detor A and Schuh C 2007 Tailoring and patterning the grain size of nanocrystalline alloys *Acta Mater.* **55** 371–9
[9] Du Y A, Ismer L, Rogal J, Hickel T, Neugebauer J and Drautz R 2011 First-principles study on the interaction of H interstitials with grain boundaries in α- and γ-Fe *Phys. Rev.* B **84** 144121
[10] Färber B, Cadel E, Menand A, Schmitz G and Kirchheim R 2000 Phosphorus segregation in nanocrystalline Ni-3.6 at% P alloy investigated with the tomographic atom probe (TAP) *Acta Mater.* **48** 789–96
[11] Geng W T, Freeman A J and Olson G B 2001 Influence of alloying additions on the impurity induced grain boundary embrittlement *Solid State Commun.* **119** 585–90
[12] Geng W, Freeman A, Wu R, Geller C and Raynolds J 1999 Embrittling and strengthening effects of hydrogen, boron, and phosphorus on a Σ5 nickel grain boundary *Phys. Rev.* B **60** 7149–55
[13] Gonze X *et al* 2002 First-principles computation of material properties: the ABINIT software project *Comput. Mater. Sci.* **25** 478–92
[14] Hammerschmidt T, Kersch A and Vogl P 2005 Embedded atom simulations of titanium systems with grain boundaries *Phys. Rev.* B **71** 205409
[15] Handtrack D, Sauer B and Kieback C 2008 Microstructure and properties of ultrafine-grained and dispersion-strengthened titanium materials for implants *J. Mater. Sci.* **43** 671–9
[16] Hohenberg P and Kohn W 1964 Inhomogeneous electron gas *Phys. Rev.* **136** B864–71
[17] Ivanov M B, Kolobov Yu R, Golosov E V, Kuz'menko I N, Veinov V P, Nechaenko D A and Kungurtsev E S 2011 Mechanical properties of mass-produced nanostructured titanium *Nanotechnol. Russia* **6** 370–8
[18] Janisch R and Elsässer C 2003 Segregated light elements at grain boundaries in niobium and molybdenum *Phys. Rev.* B **67** 224101
[19] Koch C C, Scattergood R O, Darling K A and Semones J E 2008 Stabilization of nanocrystalline grain sizes by solute additions *J. Mater. Sci.* **43** 7264–72

[20] Kohn W and Sham L J 1965 Self-consistent equations including exchange and correlation effects *Phys. Rev.* **140** A1133–8
[21] Krasko G L and Olson G B 1991 Effect of hydrogen on the electronic structure of a grain boundary in iron *Solid State Commun.* **79** 113–7
[22] Lane N, Simak S, Mikhaylushkin A, Abrikosov I, Hultman L and Barsoum M 2011 First-principles study of dislocations in hcp metals through the investigation of the (1 1 2-1) twin boundary *Phys. Rev.* B **84** 184101
[23] Lejcek P 2010 *Grain Boundary Segregation in Metals* vol 136 (Berlin: Springer)
[24] Liu K W and Mücklich F 2001 Thermal stability of nano-RuAl produced by mechanical alloying *Acta Mater.* **49** 395–403
[25] Liu L-H, Zhang Y, Hu X-L and Lu G-H 2009 Formation of a coplanar O–Al bonding cluster: the effect of O impurity on a $\Sigma = 5$ NiAl grain boundary from first-principles *J. Phys. Condens. Matter* **21** 015002
[26] Lymperakis L, Friák M and Neugebauer J 2009 Atomistic calculations on interfaces: bridging the length and time scales *Eur. Phys. J. Spec. Top.* **177** 41–57
[27] Methfessel M and Paxton A T 1989 High-precision sampling for Brillouin-zone integration in metals *Phys. Rev.* B **40** 3616–21
[28] Monkhorst H J and Pack J D 1976 Special points for Brillouin-zone integrations *Phys. Rev.* B **13** 5188–92
[29] Pellicer E, Varea A, Sivaraman K M, Pané S, Suriñach S, Baró M D, Nogués J, Nelson B J and Sort J 2011 Grain boundary segregation and interdiffusion effects in nickel-copper alloys: an effective means to improve the thermal stability of nanocrystalline nickel *ACS Appl. Mater. Interfaces* **3** 2265–74
[30] Perdew J P, Burke K and Wang Y 1996 Generalized gradient approximation for the exchange-correlation hole of a many-electron system *Phys. Rev.* B **54** 16533–9
[31] Sato Y, Mizoguchi T, Shibata N, Yamamoto T, Hirayama T and Ikuhara Y 2009 Atomic-scale segregation behavior of Pr at a ZnO [0 0 0 1] Σ49 tilt grain boundary *Phys. Rev.* B **80** 094114
[32] Sato Y, Mizoguchi T and Oba F 2005 Atomic and electronic structure of [0 0 0 1](−1 −2 3 0) Σ7 symmetric tilt grain boundary in ZnO bicrystal with linear current–voltage characteristic *J. Mater. Sci.* **40** 3059–66
[33] Sawada H 2012 First-principles study of grain boundary embrittlement in Fe–Ni–S alloy *Comput. Mater. Sci.* **55** 17–22
[34] Schweinfest R, Paxton A T and Finnis M W 2004 Bismuth embrittlement of copper is an atomic size effect *Nature* **432** 1008–11
[35] Semenova I, Salimgareeva G and Da Costa G 2010 Enhanced strength and ductility of ultrafine-grained Ti processed by severe plastic deformation *Adv. Eng. Mater.* **12** 803–7
[36] Sikka S K, Vohra Y K and Chidambaram R 1982 Omega phase in materials *Progr. Mater. Sci.* **27** 245–310
[37] Silcock J M 1958 An x-ray examination of the to phase in TiV, TiMo and TiCr alloys *Acta Metall.* **6** 481–93
[38] Tang F, Gianola D S, Moody M P, Hemker K J and Cairney J M 2012 Observations of grain boundary impurities in nanocrystalline Al and their influence on microstructural stability and mechanical behaviour *Acta Mater.* **60** 1038–47
[39] Trelewicz J and Schuh C 2009 Grain boundary segregation and thermodynamically stable binary nanocrystalline alloys *Phys. Rev.* B **79** 094112
[40] Uesugi T and Higashi K 2012 Segregation of alkali and alkaline earth metals at 11(1 1 3)[1 1 0] grain boundary in aluminum from first-principles calculations *Mater. Trans.* **53** 1699–705
[41] VanLeeuwen B K, Darling K A, Koch C C, Scattergood R O and Butler B G 2010 Thermal stability of nanocrystalline $Pd_{81}Zr_{19}$ *Acta Mater.* **58** 4292–7
[42] Wachowicz E and Kiejna A 2008 Effect of impurities on grain boundary cohesion in bcc iron *Comput. Mater. Sci.* **43** 736–43
[43] Wang Y, Li J and Ye H 1996 Structure analysis of the σ equals; 7 ((1 2 3 0)/[0 0 0 1] 21.8) grain boundary in α-Ti *Phil. Mag.* A **73** 213–22
[44] Weissmüller J, Krauss W, Haubold T, Birringer R and Gleiter H 1992 Atomic structure and thermal stability of nanostructured Y–Fe alloys *Nanostruct. Mater.* **1** 439–47
[45] Weissmüller J 1993 Alloy effects in nanostructures *Nanostruct. Mater.* **3** 261–72
[46] Zhang S, Kontsevoi O Y, Freeman A J and Olson G B 2011 First principles investigation of zinc-induced embrittlement in an aluminum grain boundary *Acta Mater.* **59** 6155–67
[47] Zhou H, Jin S, Zhang Y and Lu G 2011 First-principles study of carbon effects in a tungsten grain boundary: site preference, segregation and strengthening *Sci. China Phys. Mech. Astron.* **54** 2164–9